

PV-PCM Integration in Glazed Building. Co-Simulation and Genetic Optimization Study

Hagar Elarga^{1*}, Andrea Dal Monte², Ernesto Benini²

¹ *International Centre for Indoor Environment and Energy ICIEE, Department of Civil Engineering, Technical University of Denmark Kgs. Lyngby, 2800, Denmark*

² *Department of Industrial Engineering, University of Padua, Via Venezia 1, I-35131 Padua, Italy*

Abstract

The study describes a multi-objective optimization algorithm for an innovative integration of forced ventilated PV-PCM modules in glazed façade buildings: the aim is to identify and optimize the parameters that most affect thermal and energy performances. 1-D model, finite difference method FDM, thermal resistances technique and enthalpy method were applied to describe different façade solutions and transient thermal performance of PCM. The coupling between the PV-PCM façade code implemented in MATLAB and the TRNSYS software was developed to estimate the dynamic thermal energy profiles. An exploratory step has also been considered prior to the optimization algorithm: it evaluates the energy profiles before and after the application of PCM to PV module integrated in glazed building. The optimization analysis investigate parameters such as ventilation flow rates and time schedule to obtain the best combination suiting the PCM performance and external-internal loads. A group of solution were identified on the Pareto front. Savings in thermal loads for the best individual reached 26.4% while the best in temperature increment in operating temperatures was recorded as 6.8% comparing to the design set temperature.

Keywords: PV-PCM integrated façade, Genetic Algorithm, Optimization, TRNSYS, Thermal Numerical Simulation

*Corresponding author: Hagar Elarga
Email address: Hage1@byg.dtu.dk (Hagar Elarga¹)

1. Introduction

1.1. Background - PCM integration to PV and building sector

Although the building sector represents more than 40% of the total energy consumption in Europe (El-Sawi et al. [1]), it includes a wide range of possible solutions concerning innovative energetic technologies. PV modules integration in the building sector is one of the effective and easiest application (Machniewicz et al. [2]). The efficiency of PV modules depends on the solar radiation intensity and temperature of the panel (Ma. et al. [3]). Six basic techniques of PV thermal management could be identified: natural or forced air circulation, hydraulic or thermoelectric cooling, heat pipes and implementation of phase changing materials. Although the implementation of PCM on the back side of PV panel reduces and stabilizes its surface temperature (Pielichowska et al. [4]), the system, as a whole, needs a detailed analysis since that PCM thermal performance is depending on many uncontrolled dynamic conditions such as external temperature and wind speed (Brano et al. [5]). Elarga et al. [6] highlighted that the correct choice of the transition temperature of the PCM, coupled with a synchronized ventilation strategy for the material solidification phase, are the key features to ensure the effectiveness of the PV-PCM integration. On the other hand, there are many reported studies concerning the PCM integration in buildings in active (Li, et al. [7]) and passive systems (Elarga et al. [8]). De Gracia et al. [9] have investigated active thermal storage system TES applying a control system based on reinforcement learning technique. This proposed optimization algorithm has evaluated the system performance based on energy savings, cost reduction and CO_2 mitigation under different climates condition which obtained a more realistic evaluation concerning the building sector development.

1.2. Background - Building optimization algorithms

The analysis of the energy consumption in a building is complex and includes several parameters that could affect the performances, furthermore, the parameters to be considered in an optimization algorithm are diverse and overlapping. The necessity to implement co-simulation between different dynamic models is essential to obtain realistic results. Concerning the energy and thermal comfort performance, the optimization should include set of parameters such as the effect of climate, building architectural design, ventilation schedule and control of energy storage systems. Several novel method/design tools have been developed for aiding the

optimal building design (Lu et al. [10]). Hamdy et al. [11] proposed a modified multi-objective optimization approach which is combined with IDA ICE (building performance simulation program)[12] to minimize the investment and the equivalent CO_2 emissions for a family house including the HVAC system. Asadi et al. [13] have analyzed multiple choices for retrofitting a building implementing simulation-based multi-objective optimization scheme (a combination of TRNSYS, GenOpt and a Tchebycheff optimization technique developed in MATLAB) to optimize the retrofit cost, energy savings and thermal comfort of a residential building. GenOpt is an optimization program for the minimization of a cost function that is evaluated by an external simulation program. However, GenOpt is not capable of handling multi-objective optimization.

40 A Tchebycheff programming procedure has been developed in MATLAB to tackle the multi-objective optimization problem. A real case study is used to demonstrate the functionality of the proposed approach. The results verify the practicability of the approach and highlight that, by taking into consideration more possibilities available for building retrofit as well as more objectives for making the solving procedure extremely difficult and time-consuming.

45 Ascione et al. [14] have proposed a simulation based model predictive control (MPC) procedure (EnergyPlus and MATLAB) consisting in the multi-objective optimization for operating cost and thermal comfort of a space conditioning system. The critical issue of huge computational time, typical of simulation-based MPC, is overcome by adopting a reliable minimum run period.

Carlucci et al. [15] have implemented a multi-objective optimization to minimize thermal and visual discomfort, concluding that design procedures unsupported by automated optimization tools might find a hard challenge in exploring the entire space of variables and covering towards optimal solutions.

50 Bambrook et al. [16] conducted a design optimization using a building energy simulation program IDA ICE for a detached low energy house in the mild warm Sydney climate. The aim of the optimization was to reduce the building heating and cooling demand to the level at which the heating and cooling system was no longer necessary.

55 Wang et al. [17] investigated the optimal design solutions for zero energy building design in UK. Optimal design strategies and energy systems, including passive design parameters (external walls, window to wall ratios and orientations) and energy efficient mechanical systems as well as renewable energy systems, were provided by employing EnergyPlus and TRNSYS 16 simulation software. The weighing of the parameters on the under investigated objectives is one of the important aspects to be taken

60 into consideration during the optimization phase. Bucking et al.[18] proposed a methodology to identify the influential variations on the building performance. A back-tracking search identified

that 8 of 26 variables have significant effects on the net-energy consumption in a house case-study, especially solar orientation, variables related to the sizing of a roof-based PV system and energy-related occupant behavior. Sun [19] studied the impacts of macro-parameters of buildings and systems (such as wall thickness, window to wall ratio, system COP) and their variations in a nearly zero energy buildings (nZEB) on the system design through a systematic sensitivity analysis. He found that the indoor temperature set-point is the most significant factor in determining all building system sizes and the overall initial investment cost, followed by the system COP and internal gain intensity.

In the present work, the innovative integration of PV-PCM inside glazed facade cavity [8] has taken a step forward. The PV-PCM calculation module is integrated in an optimization loop, based on genetic algorithms. The multi-objective optimization schema has been developed on the basis of S.O.C.R.A.TE. algorithm (Dal Monte et al. [20] and [21]) in order to force the creation and mutation functions of the Matlab gamultiobj to assume integer values in part of the genetic pool. The mathematical problem results in a mixed-integer optimization where two types of design variables are considered: the ventilation schedule variables assume values in an integer domain, the mass flow variables take values in a continuous domain. The fitness functions used in the optimization represent two conflicting objectives of thermal load and thermal comfort.

2. Methodology

The objective behind the optimization analysis is to identify the best combination of investigated parameters and comprehend which of them mainly affect both the thermal loads and thermal comfort. However, it was necessary to highlight on a preliminarily basis the energy performance before and after implementing PCM to the PV integrated façades. The methodology section is subdivided into five parts. The first gives a brief introduction to the thermal resistance method, the second is discussing the PV integrated façade numerical model, the third is dedicated to the PV-PCM façade module. Following this, an illustration of how to couple the two numerical models (TRNSYS and MATLAB) is given. Finally the genetic optimization algorithm is clarified. Finite difference method FDM, fixed nodal grid and thermal resistances techniques were implemented to describe different façadessolutions under investigation.

2.1. Brief introduction to thermal resistances method

Thermal resistances R_k , R_c and R_{rad} represents respectively conduction, convection, and
 95 radiation heat transfer between the wall layers and they are determined respectively through
 Equations 1, 2, and 5.

$$R_k = x/k \quad (1)$$

where x is thickness and k is thermal conductivity.

$$R_c = 1/h_c \quad (2)$$

where h_c is the convection heat transfer coefficient.

The convection heat transfer coefficients have been evaluated by different empirical laws:
 For the outdoor surface the McAdams correlation [22] was adopted;

$$h_o = 5.62 + 3.9v \quad (3)$$

100 For the indoor layer, the convection heat transfer is evaluated using Equation 4, [23]

$$h_i = \left\{ \left[1.5 \left| \frac{\Delta T}{h_f} \right|^{0.25} \right]^6 + \left[1.23(\Delta T)^{0.33} \right]^6 \right\}^{1/6} \quad (4)$$

where ΔT is the difference between the indoor air temperature and the indoor surface
 temperature, while h_f is the floor height.

$$R_r = 1/h_r \quad (5)$$

where h_r is the radiation heat transfer coefficient.

For the radiation heat exchange, Equations 6 and 7 were used [24].

$$R_{rad} = \frac{\left(\frac{1}{\varepsilon_1} + \frac{1}{\varepsilon_2} - 1 \right)}{4\sigma(T_{avg})^3} \quad (6)$$

And hence:

$$h_r = \frac{4\sigma(T_{avg})^3}{\left(\frac{1}{\varepsilon_1} + \frac{1}{\varepsilon_2} - 1 \right)} \quad (7)$$

105 where T_{avg} is the average temperature of the two opposite surfaces, which has been evaluated
 as function of temperature previous time step values.

More details related to the numerical modelling techniques are found in [25],[26].

2.2. PV integrated façade

The exploratory step evaluates the yearly preliminary energy profiles estimated by TRNSYS
 110 between PV and PV-PCM integaretd facade. PV integrated facade grid is represented by eight
 nodes as shown in Figure 1 and the thermal resistance scheme is illustrated in Figure 2. The
 coupling of the fixed grid model developed on MATLAB to TRNSYS is further discussed in
 Section 2.4.

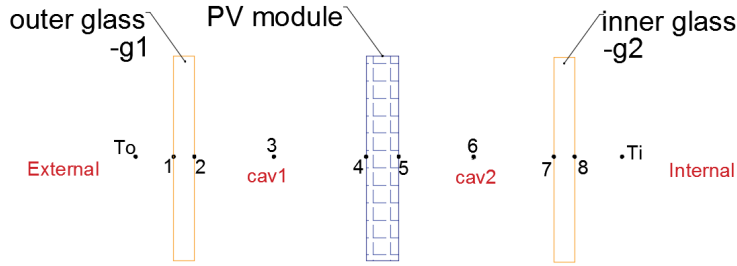


Figure 1: Representation of the PV configuration scheme.

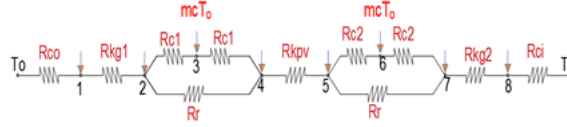


Figure 2: Representation of the RC model.

2.2.1. Description of the mathematical model

115 The mathematical model is composed by a sequence of 8 nodes, as illustrated in Figures 1
 and 2. In the external nodes 1 and 8, the heat transfer through the outer and inner layers of
 the glazed façade is described by two thermal resistances, the convection heat transfer with the
 ambient conditions and the conduction transfer within the layer itself.

$$\left(-\frac{k_{gl}}{x_{g1}} - h_o\right)T_1 + \left(\frac{k_{gl}}{x_{g1}}\right)T_2 = -I_{tr1}\left(\frac{a_{g1}}{2}\right) - (T_o h_o) \quad (8)$$

$$\left(\frac{k_{g2}}{x_{g2}}\right)T_7 + \left(-h_i - \frac{k_{g2}}{x_{g2}}\right)T_8 = -I_{tr3}\left(\frac{a_{g2}}{2}\right) - (T_i h_i) \quad (9)$$

Nodes 2, 4, 5 and 7 are representing glazed layers and PV module surfaces. Thermal resistances include thermal conductivity, thermal radiation between opposed surfaces and convection heat transfer through the ventilated cavity. The equations are:

$$\left(\frac{k_{g1}}{x_{g1}}\right)T_1 + \left(-\frac{k_{g1}}{x_{g1}} - h_{C1} - h_r -\right)T_2 + h_{C1}T_3 + h_rT_4 = -I_{tr1}\left(\frac{a_{g1}}{2}\right) \quad (10)$$

$$\left(\frac{k_{pv}}{x_{pv}}\right)T_5 + \left(-\frac{k_{pv}}{x_{pv}} - h_{C1} - h_r -\right)T_4 + h_{C1}T_3 + h_rT_2 = -I_{tr2}\left(\frac{a_{pv}}{2}\right) \quad (11)$$

$$\left(\frac{k_{pv}}{x_{pv}}\right)T_4 + \left(-\frac{k_{pv}}{x_{pv}} - h_{C2} - h_r -\right)T_5 + h_{C2}T_6 + h_rT_7 = -I_{tr2}\left(\frac{a_{pv}}{2}\right) \quad (12)$$

$$\left(\frac{k_{g3}}{x_{g3}}\right)T_8 + \left(-\frac{k_{g3}}{x_{g3}} - h_{C2} - h_r -\right)T_7 + h_{C2}T_6 + h_rT_5 = -I_{tr3}\left(\frac{a_{g2}}{2}\right) \quad (13)$$

Nodes 3 and 6 implements the energy balance of the two air cavities (*cav1* and *cav2*) which are seperated by the PV module integrated in the middle [27]. The cavities ventilation is (out to out) technique i.e. air comes form outside, ventilates the cavity and is exhausted to the outside again:

$$h_{C1}T_2 + (-2h_{C1} - \dot{m}c)T_3 + h_{C1}T_4 = -(mc)T_o \quad (14)$$

$$h_{C2}T_5 + (-2h_{C2} - \dot{m}c)T_6 + h_{C2}T_7 = -(\dot{m}c)T_o \quad (15)$$

2.3. PV-PCM model

In this subsection, the enthalpy numerical method which describes thermal performance of PCM is briefly presented. Later the energy balance equations describing the PV-PCM fixed grid model are shown. However, the enthalpy method has been previously illustrated and validated against experimental data [6]. For more details concerning the experimental campaign, reader should refer to [28].

The enthalpy method was proposed by Voller and Swaminathan [29], to model the thermal behaviour of materials undergoing a phase change, under the assumption that phase change occurs over an arbitrarily narrow temperature range. In this way, the enthalpy can be related to the temperature by a piecewise continuous function. Assuming constant specific heat capacity

in each phase, the enthalpy can be approximated using three temperature possibility ranges as in Equation 16:

$$H = \begin{cases} c_s T & \text{if } T \leq T_m - \varepsilon \\ c_s(T_m - \varepsilon) + \left[\frac{c_s + c_l}{2} + \frac{L}{2\varepsilon} \right] (T - T_m + \varepsilon) & \text{if } T_m - \varepsilon \leq T \leq T_m + \varepsilon \\ c_l T + (c_s - c_l)T_m + L & \text{if } T \geq T_m + \varepsilon \end{cases} \quad (16)$$

Where ε is an arbitrarily small value representing half the phase change temperature interval. The approximate definition $H(T)$ can be differentiated into Equation 17 with respect to temperature.

$$C^A = \frac{dH}{dT} = \begin{cases} c_s & \text{if } T \leq T_m - \varepsilon \\ \left[\frac{c_s + c_l}{2} + \frac{L}{2\varepsilon} \right] & \text{if } T_m - \varepsilon \leq T \leq T_m + \varepsilon \\ c_l & \text{if } T \geq T_m + \varepsilon \end{cases} \quad (17)$$

The definitions of $H(T)$ and C^A can be used to linearise the discretized enthalpy equation in an iterative form, as in Equation 18.

$$a_{n_b} T_{n_b} - (a_p + \rho C^A)(T_P)^n = a_p \rho C^A (T_P)^{n-1} - \rho \frac{V}{\Delta \tau} [H_p^o - H_p^{n-1}] \quad (18)$$

where H_p^o is the enthalpy node value of the previous time step, H_p^{n-1} represents the enthalpy node value of iteration $n - 1$, a are the nodal coefficients and τ is the time step.

The solution domain is defined where the derived linear equations form a matrix system, which is instantaneously solved by inverting the matrix to obtain the temperature values according to an iterative scheme. The initial values of each time step are represented by the converged solution of the previous time step. From the known temperature field and enthalpy at iteration $n - 1$, the temperatures in each node are updated. In order to ensure solution consistency, a correction and iterative loop has to be followed by saving the solution of the matrix in the previous iteration and then re-solving the system after correcting the nodal temperature T_P^n by Equation 19 with three possibilities of enthalpy ranges until the convergence is reached. The

code thus saves the calculated temperature field, and starts a new time step.

$$T_P^n = \begin{cases} \left(\frac{H_P^n}{c_s} \right) & \text{if } H_P^n \leq c_s(T_m - \epsilon) \\ \left(\frac{H_P^n + \left[\frac{c_s + c_l}{2} + \frac{L}{2\epsilon} \right] (T_m - \epsilon)}{c_s + c_l + \frac{L}{2\epsilon}} \right) & \text{if } c_s(T_m - \epsilon) \leq H_P^n \leq c_s(T_m + \epsilon) \\ \frac{H_P^n - (c_s - c_l)T_m - L}{c_l} & \text{if } H_P^n \geq c_s(T_m + \epsilon) + L \end{cases} \quad (19)$$

2.3.1. Description of the mathematical model

155 In the PV-PCM mathematical model a scheme composed by 15 nodes is adopted, as shown in Figures 3 and 4.

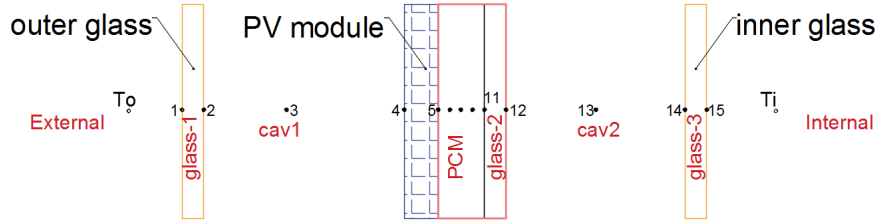


Figure 3: Representation of the PV-PCM facade configuration scheme.

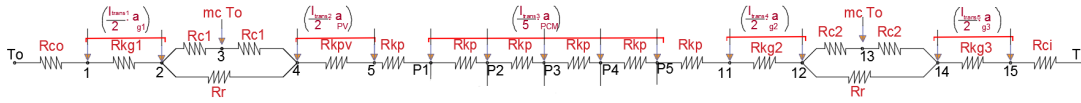


Figure 4: Representation of the RC scheme.

Thermal conduction and convection resistances are moderating the thermal performance of the external nodes 1 and 15.

$$\left(-\frac{K_{gl}}{x_{g1}} - h_o \right) T_1 + \left(\frac{K_{gl}}{x_{g1}} \right) T_2 = -I_{tr1} \left(\frac{a_{g1}}{2} \right) - (h_o T_o) \quad (20)$$

$$\left(-\frac{K_{g3}}{x_{g3}} - h_i \right) T_{15} + \left(\frac{K_{gl}}{x_{g1}} \right) T_{14} = -I_{tr5} \left(\frac{a_{g1}}{2} \right) - (h_i T_i) \quad (21)$$

Radiation heat exchange between surfaces is appeared in the energy balance between nodes
 160 2, 4 and between 12 and 14.

$$\left(\frac{K_{g1}}{x_{g1}}\right)T_1 + \left(-\frac{K_{gl}}{x_{g1}} - h_{C1} - h_r\right)T_2 + h_{C1}T_3 + h_rT_4 = -I_{tr1}\left(\frac{a_{g1}}{2}\right) \quad (22)$$

$$h_rT_2 + h_{C1}T_3 + \left(-h_r - h_{C1} - \frac{k_{pv}}{x_{pv}}\right)T_4 + \left(\frac{k_{pv}}{x_{pv}}\right)T_5 = -I_{tr2}\left(\frac{a_{pv}}{2}\right) \quad (23)$$

$$\left(\frac{k_{g2}}{x_{g2}}\right)T_{11} + \left(-h_r - h_{C2} - \frac{k_{g2}}{x_{g2}}\right)T_{12} + h_{C2}T_{13} + h_rT_{14} = -I_{tr4}\left(\frac{a_{g2}}{2}\right) \quad (24)$$

$$\left(\frac{K_{g3}}{x_{g3}}\right)T_{15} + \left(-\frac{K_{g3}}{x_{g3}} - h_{C2} - h_r\right)T_{14} + h_{C2}T_{13} + h_rT_{12} = -I_{tr5}\left(\frac{a_{g3}}{2}\right) \quad (25)$$

Forced convection was implemented within both cavities represented by node 3 and 13.

$$h_{C1}T_2 + (-2h_{C1} - \dot{m}c)T_3 + h_{C1}T_4 = -(\dot{m}c)T_o \quad (26)$$

$$h_{C2}T_{12} + (-2h_{C2} - \dot{m}c)T_{13} + h_{C2}T_{14} = -(\dot{m}c)T_o \quad (27)$$

In Nodes 5 and 11 thermal conductivity is the only heat transfer mode dominating the energy balance.

$$\left(\frac{k_{pv}}{x_{pv}}\right)T_4 + \left(-\frac{k_{pv}}{x_{pv}} - \frac{k_{p1}}{x_{p1}}\right)T_5 + \left(\frac{k_{p1}}{x_{p1}}\right)T_{p1} = -I_{tr2}\left(\frac{a_{pv}}{2}\right) \quad (28)$$

$$\left(\frac{k_{p5}}{x_{p5}}\right)T_{p5} + \left(-\frac{k_{p5}}{x_{p5}} - \frac{k_{g2}}{x_{g2}}\right)T_{11} + \left(\frac{k_{g2}}{x_{g2}}\right)T_{12} = -I_{tr4}\left(\frac{a_{g2}}{2}\right) \quad (29)$$

Each homogeneous sub layer from the five nodes composing PCM layer (nodes from P1 to
 165 P5, as shown in Figure 4) is represented by a conductive resistance and an enthalpy term, for the sake of brevity; clarified only one node thermal balance node P2, in Equation 30:

$$\begin{aligned} &\left(\frac{k_p}{x_p}\right)T_{p1} + \left(-2\frac{k_p}{x_p} - \frac{\rho x_p (c^A)_{p2}}{\Delta\tau}\right)T_{p2} + \left(\frac{k_p}{x_p}\right)T_{p3} = \\ &-I_{tr3}\left(\frac{a_{pcm}}{2}\right) + \left(\frac{\rho x_p (c^A)_{p2}}{\Delta\tau}\right)^{n-1} T_{p2}^{n-1} - \rho \frac{x_p}{\Delta\tau} [H_P^0 - H_P^{n-1}] \end{aligned} \quad (30)$$

2.4. MATLAB-TRNSYS coupling

In order to obtain a reliable simulation of the impact of a PV-PCM combination on the building energy demand, a yearly thermal loads analysis has to be clarified. The previously presented PV-PCM 1-D model developed in MATLAB has to be linked to TRNSYS (Klein et al. [30]). TRNSYS is a dynamic thermal model that takes into account both the external and internal loads and the stored heat in the building components. The interaction between MATLAB and TRNSYS Simulation Studio has been carried out using TYPE155 from TRNYS library. This type is dedicated to read external codes executed by MATLAB. The numerical algorithm starts by linking the required weather condition from TYPE16 to both the MATLAB and the zone built in TRNbld TYPE56. Generally, it is mandatory to link the weather file to TYPE56 in order to operate the simulation model . On the other hand, for each listed inner zone on TYPE56, there is availability to set its input data and boundary conditions as a user defined option. The PV-PCM -1D numerical code estimates the temperature and transmitted solar radiation for each of the fixed grid nodes including the last node which represents the inner surface layer temperature i.e. node 15. However, the transient interface between TRNSYS and MATLAB models occurs in air node 13 (see Figure 4). The estimated transmitted solar radiation and air temperature with a 15 minutes time step are read as a user defined value for the inner layer zone on TYPE56. The reason behind considering the coincident interface between the two models in node 13 is that to obtain the correct inner glazed surface energy balance and its final temperature, the complete room structure and the correspondent radiative/convective heat exchange between all room inner surfaces(which includes also thermal storage of the room walls) have to be considered. The inner glass layer has been identified in TRNbld TYPE56 library with the specifications of Table 1.

190

Density	2500 kg/m^3
Capacity	0.84 $kJ/(kgK)$
Conductivity	0.27 $kJ/(hmK)$

Table 1: Glazed layer specifications

The inside set temperatures, adopted in the analysis, for the summer and winter seasons are defined in Table 2. The considered façade is west oriented and the office area is $80m^2$ and

internal loads were evaluated as $24W/m^2$.

	Period	Working days	Weekend
Cooling season	Working hours (07:00 19:00)	25°C	29°C
	Idle hours (19:00 07:00)	32°C	32°C
Heating season	Working hours (07:00 19:00)	20°C	17°C
	Idle hours (19:00 07:00)	15°C	15°C

Table 2: Inside Set Temperature

2.5. Genetic Algorithm Optimization

195 Genetic algorithms represent one of the most powerful tool to analyse problems characterized by the influence of several parameters that lead to the definition of multiple optimal solutions. The representation of the optimization schema adopted for the proposed analysis is shown in Figure 5. The overall optimization is lead by MATLAB gamultiobj algorithm; the genes represent the parameters for the PV-PCM façade calculation (carried in MATLAB) and the resulting distributions of the cavity air node temperature T_{ac} , thermal energy Q_{th} and cavity convection heat transfer coefficient h_c are saved. The inner zone calculation, implemented in the TRNSYS module, uses the previous distributions in order to evaluate the thermal load Q_{th} and the operating temperature T_{op} evolutions in each time step of the year. In the second MATLAB module, different in-house functions elaborate the data in order to determine two
200
205 single parameter value to describe the performances of the individual.

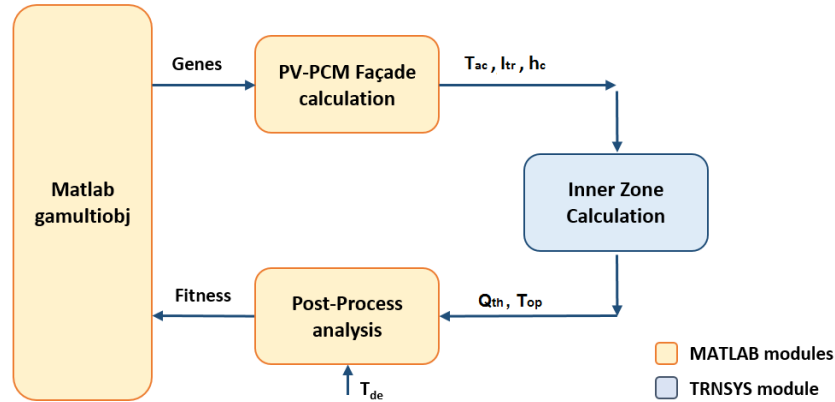


Figure 5: Schematic representation of the genetic algorithm.

The population adopted for optimization consists of 40 individuals composed by a set of 8 genes; the optimization run for a total number of 50 generations. The first population considered in the algorithm is random initialized.

2.5.1. Design Variables

210 In the optimization terminology, an *individual* represents the codification of a certain setting of the analysis and the resulting performances are calculated starting from its parameters; furthermore, the individual's *chromosome* consists of the sequence of parametric values to be optimized.

In the present optimization, the considered design variables (defined with the X array, 215 illustrated in Table 3) determines the schedule of the ventilation inside the two cavities; genes $X(1)$ and $X(2)$ represent the mass flow values multiplied by the air specific heat capacity (mc_{p1} and mc_{p2} in $[J/sK]$), in genes from $X(3)$ to $X(5)$ the starting hour of the ventilation system is fixed for Winter, Mid-Seasons and Summer; finally genes from $X(6)$ to $X(8)$ establish the duration of the ventilation during the three periods. The parameters that determine the 220 schedules of ventilation are represented by an integer number: the values are further converted in a starting hour or a duration using a factor of 30 minutes. For instance, the ventilation in winter of the baseline individual (3rd row of Table 3) starts at 8.00a.m. ($16 * 0.5h$, Gene $X(3)$) and is turned off after 8 hours ($16 * 0.5h$, Gene $X(3)$).

	X(1)	X(2)	X(3)	X(4)	X(5)	X(6)	X(7)	X(8)
Lower Bounds	60	60	0	0	0	0	0	0
Upper Bounds	360	360	48	48	48	20	20	20
Baseline	100	100	16	16	16	16	16	16

Table 3: Upper and lower bounds adopted for the design variables, chromosome of the baseline individual considered for the optimization.

2.5.2. Objective Functions and Constraints

225 The optimization problems concerns the minimization of two conflicting objective functions. The first objective function f_Q is represented by the ratio between the total thermal load of a

year, of the considered individual and the baseline setting, calculated as:

$$f_Q = \frac{\sum_{i=1}^n |Q_{th,i}|}{Q_{th,bas}} \quad (31)$$

The thermal comfort $f_{\Delta T}$ is the second objective function. In the present formulation, it is defined as the differences between the calculated operating temperature T_{op} and the desired design temperature T_{de} . The value is normalized with respect the value of the baseline configuration:

$$f_{\Delta T} = \frac{\sum_{i=1}^n |T_{op,i} - T_{de,i}|}{\Delta T_{bas}} \quad (32)$$

Furthermore, a linear inequality constraint is set in order to limit the sum of mass flow rate multiplied by the air specific heat capacity mc_p in cavities 1 and 2 to $400 J.s^{-1} K^{-1}$, i.e $0.4 kg.s^{-1}$.

$$X(1) + X(2) \leq 400 \quad (33)$$

The choice of using two contrasting functions allows to determine a Pareto front and to identify several solutions, based on the importance given to the considered objectives.

3. Results and Discussion

The results are divided into two main sections; first, the baseline configuration with and without PCM is presented in order to highlight the effect of PCM on the performance, the second section contains the results of the optimization and different individuals belonging to the Pareto Front are analysed.

3.1. Exploratory analysis: PV with and without PCM integrated façade

For a complete test reference year data TRY, two simulations were run considering cases with and without PCM. Ventilation air flow rate for both cavities were considered $10 l/s$ per façade meter [31], [32] and it was ON during working hours, which started from 7.00 to 19.00. The inside set temperatures have been previously specified in Table 2.

Thermal analysis has been investigated for both cases to highlight the influence of the PCM latent heat storage capability. In Figure 6 the thermal energy profile for the week of 16th – 23th of July is presented; in fact, according to the TRY database, this month is recorded as the

250 hottest month in Venice summer season. As it is shown, thermal cooling loads are always higher during the day working hours. The implementation of PCM reduced thermal cooling loads all over the summer season by 48 %.

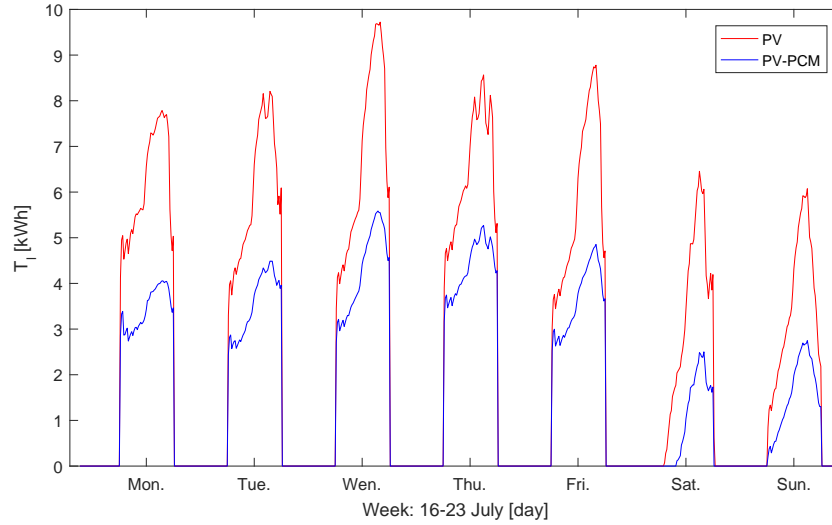


Figure 6: Week thermal energy profiles.

This initial exploratory study is followed by the optimization analysis to determine which are the parameters that influence on the PCM performance.

255 3.2. Optimization Analysis

3.2.1. Analysis of Genetic Algorithm results

The results of the optimization of the PV-PCM façade configuration are presented in terms of Pareto front analysis. The evolution of the Pareto front through the generation is shown in Figure 7: as can be noticed, the genetic algorithm greatly improved the performances of the individual until the 30th generation, after that, the convergence seems to be reached and no further improvements are found. On the other hand, Figure 8 presents the overall Pareto front of the optimization, considering all the analysed individuals.

Individuals belonging to the front represent the best solutions in, at least, one objective function of the optimization. A single solution can not be considered as the best configuration, hence several individuals distributed along the front are hereby analysed. Table 4 compares the genetic pools and the fitness values of the considered individuals belonging to the Pareto front and the baseline configuration.

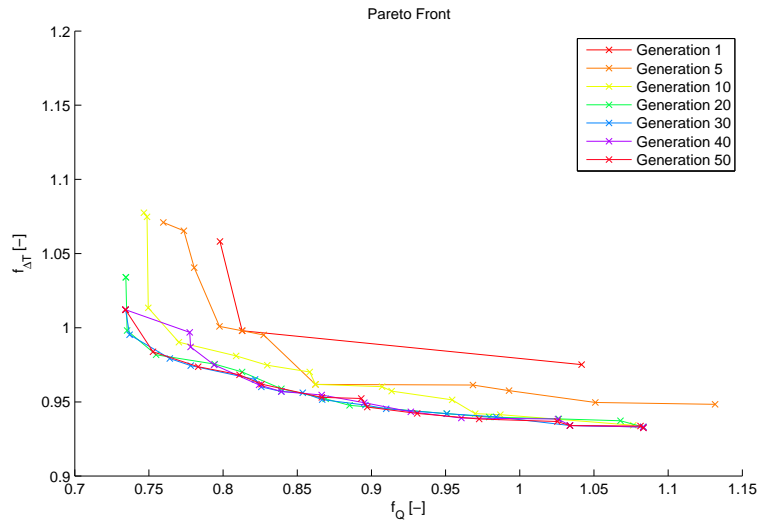


Figure 7: Evolution of the Pareto front through the generations.

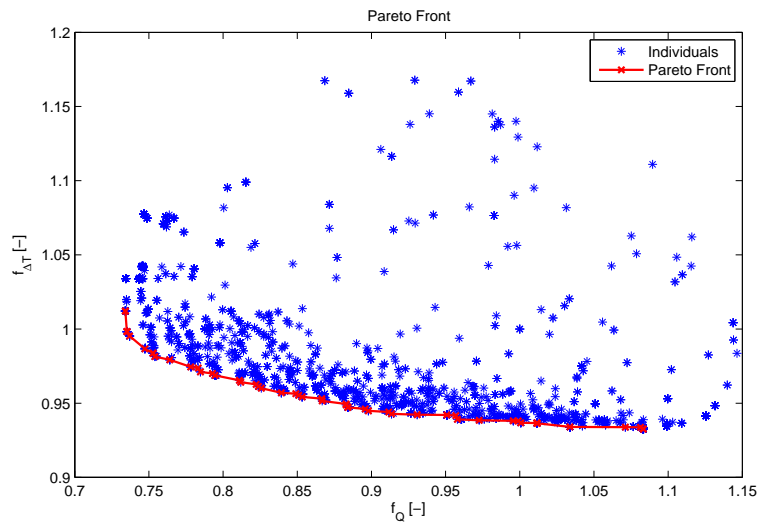


Figure 8: Final Pareto front of the optimization.

The first solutions to be discussed are located in the upper-left part of the Pareto front, they represent the best configuration for the thermal load reduction with no significant improvements in the thermal comfort (Figure 9). The setting of *Ind01* allows the greatest reduction in the thermal load f_Q (-26.4%), however $f_{\Delta T}$ has been slightly increased of 1.2%. *Ind02* presents similar performances in terms of f_Q with *Ind01* and almost the same $f_{\Delta T}$ of the baseline. It is

	X(1)	X(2)	X(3)	X(4)	X(5)	X(6)	X(7)	X(8)	f_Q	$f_{\Delta T}$
Basel.	100.00	100.00	16	16	16	16	16	16	1.000	1.000
Ind01	158.25	106.96	13	19	15	1	16	20	0.734	1.012
Ind02	166.61	104.81	11	20	15	2	17	20	0.735	0.998
Ind03	186.37	106.12	9	19	15	4	19	19	0.754	0.981
Ind04	186.11	106.74	9	19	15	5	19	17	0.785	0.971
Ind05	181.54	106.42	10	19	15	4	19	14	0.826	0.960
Ind06	183.76	106.75	10	19	15	4	19	11	0.867	0.951
Ind07	176.60	106.58	10	19	15	5	19	6	0.958	0.939
Ind08	162.41	106.11	15	18	16	11	20	5	1.083	0.932

Table 4: Genetic pool and fitness values of the considered individuals belonging to the Pareto front.

interesting to notice how the greatest reductions in thermal load have been obtained with the limitation of the ventilation time in winter season to 1 and 2 hours; it can be concluded the ventilation in winter is not necessary to improve the thermal load performance.

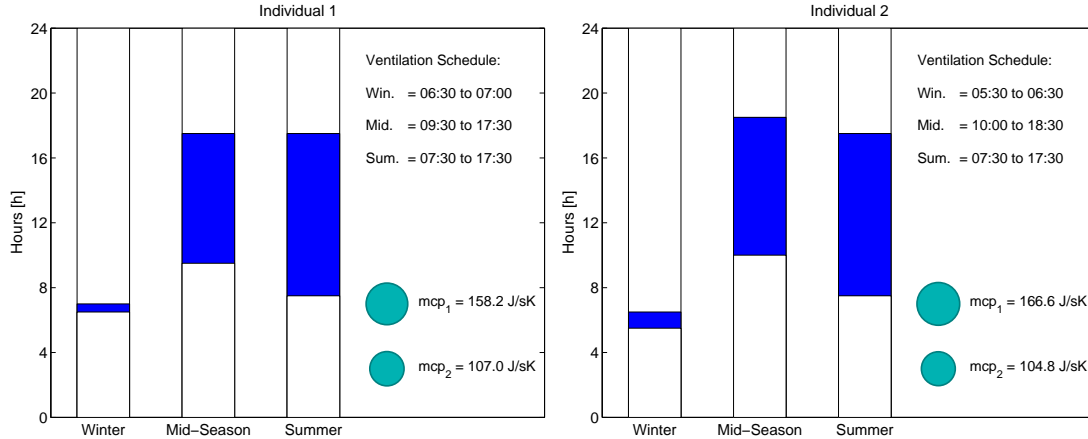


Figure 9: Graphical representation of the schedule of Individuals 1 (on the left) and 2 (on the right).

Moving along the Pareto Front towards right, the solutions improve the performances in terms of $f_{\Delta T}$ and at the same time get worse considering f_Q . Great increments in thermal load can be observed for *Ind03* (-24.6%) and *Ind04* (-21.5%) with small improvements in $f_{\Delta T}$ (Figure 10). As can be seen in Figure 11, improvements in thermal load are reduced for *Ind05* (-17.4%)

280 and *Ind06* (-13.3%) however the thermal comfort increases, being the operating temperature closer to the design temperature (decrease of 4.0% and 4.9% in $f_{\Delta T}$).

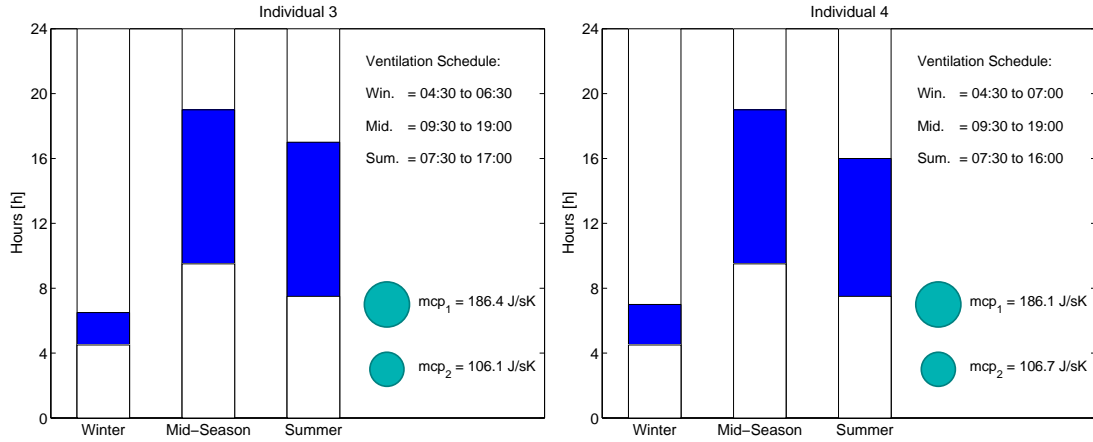


Figure 10: Graphical representation of the schedule of Individuals 3 (on the left) and 4 (on the right).

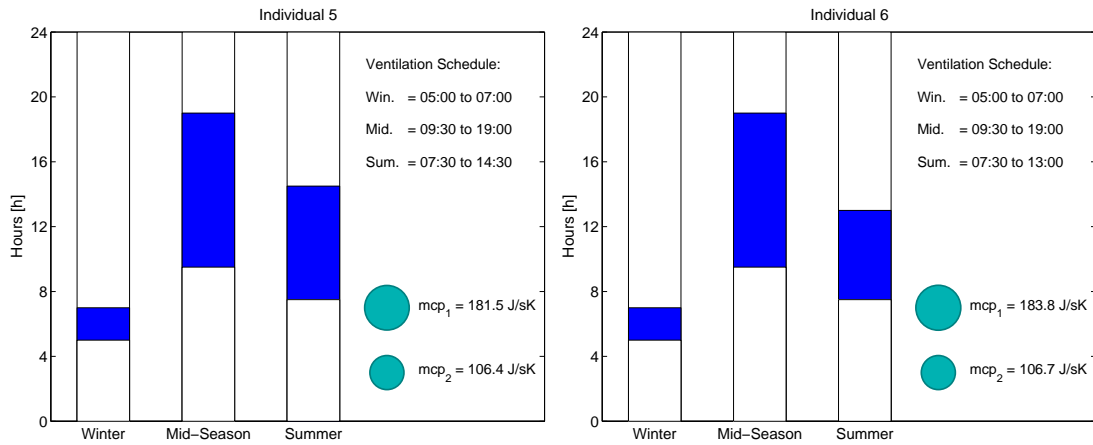


Figure 11: Graphical representation of the schedule of Individuals 5 (on the left) and 6 (on the right).

Finally, the last two considered individuals are found in the down-right zone of the Pareto Front (Figure 12). *Ind07* improves $f_{\Delta T}$ of 6.1% with a limited reduction of thermal load of 4.2%. The best individual of the optimization for the reduction of $f_{\Delta T}$ (- 6.8%) is represented by *Ind08*, however its performance, in terms of f_Q , is decreased compared to the baseline, with an increment in thermal load of 8.3%.

Some considerations can also be done observing the trend of parameters along the Pareto

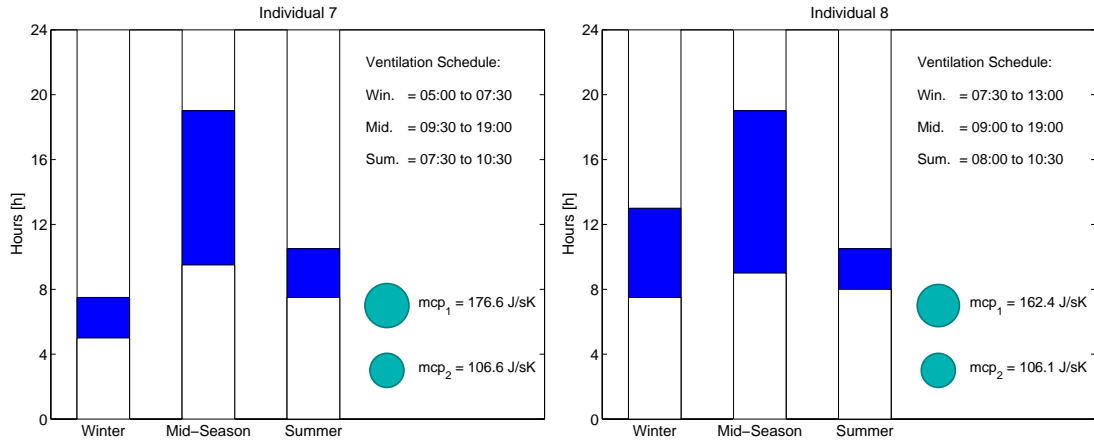


Figure 12: Graphical representation of the schedule of Individuals 7 (on the left) and 8 (on the right).

front (from *Ind01* to *Ind08*). The progressive slightly increment in the duration of ventilation during the Winter season is opposed to the marked decrease in the Summer season. In the meanwhile the values of mass flow of *cav1*, increase with respect *Ind01* and *Ind02*. A clear trend in the parameters can be identified: thermal load can be reduced by limiting the ventilation in winter and increasing its duration in summer; on the other hand if thermal comfort is the primary goal, the ventilation should be reduced in summer and increased during winter season.

3.2.2. PV-PCM Integration Air Thermal Analysis

The eight individuals analysed from Figure 9 to 12 are reflecting the thermal performances of the optimization different solutions. Considering *Ind01*, during the winter season both cavities *cav1* and *cav2* were almost not ventilated. It was enough to depend on the PCM latent heat storage capability. However, the pattern has changed during both the summer and mid seasons. In the mid-season, the cavity ventilation started in 9:30 am and lasted for 8 hours while in the summer season, the ventilation started in 7:30 am and lasted till 17:30 pm. This ventilation schedule has enforced the PCM charging/discharging process efficiently to confront the external and internal loads, in which the PCM works under its highest values of specific heat capacity. With almost the same ventilation schedule in *Ind02*, the first fitness function i.e. thermal loads has not improved much. On the other hand, by reducing the summer ventilation time period, thermal loads started to increase more. The ventilation flow rates as a whole were considered not to exceed 16l/s per façade meter.

The influence of ventilating *cav1* is higher on the required thermal loads in comparing to *cav2*. The ventilation flow rate of *cav2* is almost constant and equal to 4.5 l/s per façade meter in all seasons while in *cav1* it ranged between 6 to 8 l/s per façade meter. This indicates that higher flow rates implemented to cool the PV surface is improving the overall energy balance of the inner zone. On the other hand, PCM requires lesser mass flow rates in respect to its variable physical states and thermal inertia. In Figure 13, the energy profiles for three individuals (*Ind01*, *Ind05* and *Ind08*) are compared. The required cooling loads in *Ind01* is in between the range of 2 and 4 kWh till almost 18 h and it increases to 5 kWh which confront the ventilation termination of cavity 2. The same profile occurred in the other cases; however the thermal requirements rises in 15 h in *Ind03* and in 11 h in *Ind08*. Which again confirming the importance of the cavity ventilation schedule.

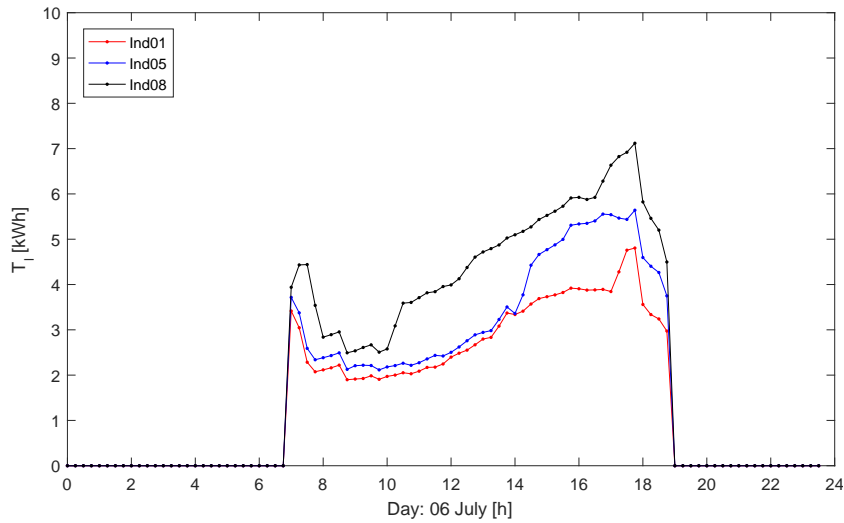


Figure 13: 6th July: comparison of daily thermal energy profiles for different solutions.

4. Conclusions

The objective of the study is to highlight that not only energy trends and savings are essential to evaluate the success of innovative applications, but also the thermal comfort has to be taken into account. The multi-objective optimization study allowed to identify a set of solutions between the best in thermal loads and best in thermal comfort; accordingly, a compromise decisions to ensure both energy savings and indoor comfort has to be made.

The results demonstrates how both the schedule of ventilation and air flow rates represent
325 key parameters for the optimization: the thermal energy requirements were reduced and
the maximum advantage of the implemented PCM layer was obtained. Thermal loads are
proportional to ventilation starting hour and duration, especially during the cooling season.
When the duration dropped below 7 hours, the required thermal loads started to deteriorate.
High solar radiation, intensity and external temperature need the ventilation system to support
330 the PCM solidification process. During winter season, heating loads were inverse proportional to
the cavities ventilation. The best thermal performance solution was obtained by not ventilating
the cavities. This is due to the low external loads, accordingly the PCM is almost working under
its solid states. On the other hand, the second fitness function concluded in the difference
between design and the operating inside temperatures has a different trend. This temperature
335 difference is inverse proportional to the cavities ventilation duration. In the summer season;
not ventilating the cavity is delaying the PCM solidification phase. Thus, the PCM latent heat
storage capability, which produce a more flatter temperature profile, is in its minimum level
i.e. specific heat capacity is $2kJkg^{-1}K^{-1}$. Finally, to expand the study on urban scale, it is
important to highlight that the PCM type has to be properly selected to suit the boundary
340 conditions of each case under investigation.

Further works should also focus on the economical considerations to expand the results on
urban scale deployment. In fact, the cost of energy definitely represents a main factor and a
third contrasting objective to be taken into account during the decision process regarding the
implementation of a PV-PCM module.

345 **Nomenclature**

a	Solar absorption coefficient	–
c_l	PCM Liquid specific heat capacity	J/kgK
c_s	PCM Solid specific heat capacity	J/kgK
C^A	Heat Capacity	J/kgK
h	Convection heat transfer coefficient	W/m^2K
h_c	Air cavity convection heat transfer coefficient	W/m^2K
H	Enthalpy	J/kg
H_P	Enthalpy node value	J/kg
f_h	Floor height	m
f_Q	Thermal load fitness	–
$f_{\Delta T}$	Operating temperature fitness	–
i	Iteration number	–
L	Latent heat storage	J/kgK
\dot{m}	Mass flow rate	kg/s
n	Maximum iteration number	–
I_{tr}	Transmitted solar radiation	$kW.h$
Q_{th}	Thermal load	$kW.h$
$Q_{th,bas}$	Thermal load of baseline individual	$kW.h$
t	Time	s
T	Temperature	K
T_{ac}	Temperature of air cavity	K
T_{de}	Design temperature	K
T_m	Melting peak temperature	K
T_{nb}	Adjacent nodes Temperature	K
T_{op}	Operating temperature	K
T_P	PCM node Temperature	K
k	Thermal conductivity coefficient	W/mK
R	Thermal Resistance	m^2K/W
v	Air velocity	m/s
X	Vector of Genes	–

ΔT_{bas}	Temperature difference in baseline individual	$^{\circ}C$
ε	Arbitrary small temperature value	K
ρ	Mass density	kg/m^3
τ	Time step	s

Acronyms

<i>HVAC</i>	Heating Ventilation and Air Conditioning
<i>PCM</i>	Phase Change Material
<i>PV</i>	Photo Voltaices
<i>nZEB</i>	nearly Zero Energy Building

References

- [1] A. El-Sawi, F. Haghghat, and H. Akbari, "Assessing long-term performance of centralized thermal energy storage system," *Applied Thermal Engineering*, vol. 62, no. 2, pp. 313–321, 2014.
- [2] A. Machniewicz, D. Knera, and D. Heim, "Effect of transition temperature on efficiency of pv/pcm panels," *Energy Procedia*, vol. 78, pp. 1684–1689, 2015.
- [3] T. Ma, H. Yang, Y. Zhang, L. Lu, and X. Wang, "Using phase change materials in photovoltaic systems for thermal regulation and electrical efficiency improvement: A review and outlook," *Renewable and Sustainable Energy Reviews*, vol. 43, pp. 1273–1284, 2015.
- [4] K. Pielichowska and K. Pielichowski, "Phase change materials for thermal energy storage," *Progress in materials science*, vol. 65, pp. 67–123, 2014.
- [5] V. L. Brano, G. Ciulla, A. Piacentino, and F. Cardona, "Finite difference thermal model of a latent heat storage system coupled with a photovoltaic device: Description and experimental validation," *Renewable Energy*, vol. 68, pp. 181–193, 2014.
- [6] E. B. Hagar Elarga, Francesco Goia, "Pv-pcm integration in glazed buildings. numerical study through matlab/trnsys linked model." in *Building Simulation Application conference, Bolzano Italy*, vol. 3, 2017, p. 8.

- [7] G. Li, Y. Hwang, and R. Radermacher, “Review of cold storage materials for air conditioning application,” *International Journal of Refrigeration*, vol. 35, no. 8, pp. 2053–2077, 2012.
- [8] H. Elarga, F. Goia, A. Zarrella, A. Dal Monte, and E. Benini, “Thermal and electrical performance of an integrated pv-pcm system in double skin façades: A numerical study,” *Solar Energy*, vol. 136, pp. 112–124, 2016.
- [9] A. d. Gracia Cuesta, R. Barzin, C. Fernández Camon, M. M. Farid, and L. F. Cabeza, “Control strategies comparison of a ventilated facade with pcm–energy savings, cost reduction and co2 mitigation,” *Energy and Buildings*, 2016, vol. 130, p. 821–828, 2016.
- [10] Y. Lu, S. Wang, and K. Shan, “Design optimization and optimal control of grid-connected and standalone nearly/net zero energy buildings,” *Applied Energy*, vol. 155, pp. 463–477, 2015.
- [11] M. Hamdy, A. Hasan, and K. Siren, “Applying a multi-objective optimization approach for design of low-emission cost-effective dwellings,” *Building and environment*, vol. 46, no. 1, pp. 109–123, 2011.
- [12] H. Analysis and T. Kalamees, “Ida ice: the simulation tool for.”
- [13] E. Asadi, M. G. da Silva, C. H. Antunes, and L. Dias, “A multi-objective optimization model for building retrofit strategies using trnsys simulations, genopt and matlab,” *Building and Environment*, vol. 56, pp. 370–378, 2012.
- [14] F. Ascione, N. Bianco, C. De Stasio, G. M. Mauro, and G. P. Vanoli, “Simulation-based model predictive control by the multi-objective optimization of building energy performance and thermal comfort,” *Energy and Buildings*, vol. 111, pp. 131–144, 2016.
- [15] S. Carlucci, G. Cattarin, F. Causone, and L. Pagliano, “Multi-objective optimization of a nearly zero-energy building based on thermal and visual discomfort minimization using a non-dominated sorting genetic algorithm (nsga-ii),” *Energy and Buildings*, vol. 104, pp. 378–394, 2015.
- [16] S. Bambrook, A. Sproul, and D. Jacob, “Design optimisation for a low energy home in sydney,” *Energy and Buildings*, vol. 43, no. 7, pp. 1702–1711, 2011.

- [17] L. Wang, J. Gwilliam, and P. Jones, “Case study of zero energy house design in uk,” *Energy and buildings*, vol. 41, no. 11, pp. 1215–1222, 2009.
- [18] S. Bucking, R. Zmeureanu, and A. Athienitis, “A methodology for identifying the influence of design variations on building energy performance,” *Journal of Building Performance Simulation*, vol. 7, no. 6, pp. 411–426, 2014.
- [19] Y. Sun, “Sensitivity analysis of macro-parameters in the system design of net zero energy building,” *Energy and Buildings*, vol. 86, pp. 464–477, 2015.
- [20] A. Dal Monte, M. R. Castelli, and E. Benini, “Multi-objective structural optimization of a hawt composite blade,” *Composite Structures*, vol. 106, pp. 362–373, 2013.
- [21] A. Dal Monte, S. De Betta, M. R. Castelli, and E. Benini, “Proposal for a coupled aerodynamic–structural wind turbine blade optimization,” *Composite Structures*, vol. 159, pp. 144–156, 2017.
- [22] H. C. Hottel and W. McAdams, “Heat transmission,” 1954.
- [23] I. Beausoleil-Morrison, *The adaptive coupling of heat and air flow modelling within dynamic whole-building simulation*. University of Strathclyde UK, 2000.
- [24] Y. Çengel, “Heat and mass transfer, a practical approach,” *New York*, 2007.
- [25] H. Elarga, M. De Carli, and A. Zarrella, “A simplified mathematical model for transient simulation of thermal performance and energy assessment for active facades,” *Energy and Buildings*, vol. 104, pp. 97–107, 2015.
- [26] M. De Carli, H. Elarga, A. Zarrella, and M. Tonon, “Evaluation of energy recovery of multiple skin facades: The approach of digithon,” *Energy and Buildings*, vol. 85, pp. 337–345, 2014.
- [27] H. Elarga, A. Zarrella, and M. De Carli, “Dynamic energy evaluation and glazing layers optimization of facade building with innovative integration of pv modules,” *Energy and Buildings*, vol. 111, pp. 468–478, 2016.
- [28] F. Goia, M. Perino, and M. Haase, “A numerical model to evaluate the thermal behaviour of pcm glazing system configurations,” *Energy and Buildings*, vol. 54, pp. 141–153, 2012.

- [29] V. Voller, “An overview of numerical methods for solving phase change problems,”
420 *Advances in numerical heat transfer*, vol. 1, no. 9, pp. 341–380, 1997.
- [30] S. Klien, W. Beckman, J. Mitchell, J. Duffie, N. Duffie, T. Freeman, J. Mitchell, J. Braun,
B. Evans, J. Kummer *et al.*, “Trnsys 16—a transient system simulation program, user
manual,” *Solar Energy Laboratory. Madison, WI: University of Wisconsin-Madison*, 2004.
- [31] J. Parra, A. Guardo, E. Egusquiza, and P. Alavedra, “Thermal performance of ventilated
425 double skin façades with venetian blinds,” *Energies*, vol. 8, no. 6, pp. 4882–4898, 2015.
- [32] M. Kragh, “Monitoring of advanced facades and environmental systems,” *whole-life
performance of facades University of Bath, CWCT*, 2001.